Traversing Scales of Brain and Behavioral Organization II: Analysis and Reconstruction

Armin Fuchs, Viktor K. Jirsa, and J.A. Scott Kelso

Program in Complex Systems and Brain Sciences, Center for Complex Systems, Florida Atlantic University, 777 Glades Road, Boca Raton, FL 33431, USA

1 Introduction: Probing the Human Brain

Brain signals can be recorded from humans in a great variety of experimental setups and task conditions. As outlined in the first of our papers (Kelso, Fuchs and Jirsa this volume, referred to in the following as KFJ) our approach aims at specific situations were (in most cases) coordination tasks are used to prepare the brain into a certain state. Changing this state by either the variation of an external parameter or slight changes in the task allows us to link properties of movement behavior to ongoing neural activity. In so-called transition paradigms we have shown how the spatiotemporal patterns obtained by recordings of the electric scalp potential (EEG) (Wallenstein et al. 1995), (Meaux et al. 1996) or the magnetic field (MEG) (Fuchs et al. 1992) undergo changes when spontaneous switches in the subject's motor coordination occur. Here we describe in detail how analysis and visualization techniques can be used to show how brain activity is related to a kinematic feature of finger movement – its velocity profile, as outlined in KFJ. We are going to show which parts of the brain signals are invariant a cross different movement types, i.e. the flexion or extension of an index finger, and what differences can be found for different task conditions, i.e. syncopation or synchronization with an external stimulus.
This paper is organized as follows:

- Sect. 2 gives a brief overview about the state of the art technology for (noninvasive) recordings from the human brain and it summarizes the advantages and disadvantages of different methods. We also briefly review the visualization and analysis techniques we are going to apply to the experimental data;
- Sect. 3 presents the results; and
- Sect. 4 contains the conclusions and some future perspectives.

2 Recording Technology, Visualization, and Analysis

2.1 Technology

One of the goals in brain research is to find the spatial distribution of electric current density $\mathbf{j}(\mathbf{r}, t)$ inside the brain at each moment in time. In a perfect

C. Uhl (ed.), *Analysis of Neurophysiological Brain Functioning*

situation this distribution could be measured from the outside and, knowing all the inputs, could be predicted from a "brain theory". Unfortunately, the problem of calculating the current density inside a volume from measurements on a surface outside this volume (known as the "inverse problem") is ill-posed, i.e., it has no unique solution. There are essentially two methods in use to record the electric and magnetic activity of the human brain that are purely non-invasive:

Electroencephalography (EEG) records the electric potential at the scalp surface from typically a few (in clinical applications) to up to about 200 (in research labs) different locations. The electric potential is a quantity that can only be measured with respect to a reference (i.e., only potential differences can actually be measured). It has always been an issue what is a "good" reference because different locations of the reference electrode lead to different spatial patterns of the electric potential, and what is the "best" reference procedure is mostly a philosophical issue (see e.g. Nunez (1981) for a detailed discussion of the physics of this problem). Moreover, EEG signals are contaminated and smeared due to electric volume conduction inside the brain tissue and cerebral fluid before they reach the scalp leading to different activity patterns on the scalp versus the cortex. There are different techniques in use to deblur these signals. One common method is calculating spatial derivatives (Laplacians, which also solves the reference problem because this quantity is independent of the reference used) (Nunez et al. 1993). It is also possible to estimate the local conductivity of the tissue from MRI scans (Le and Gevins 1993), and calculate the current density on the surface of the cortex;

Magnetoencephalography (MEG). Most of today's magnetometers measure the radial component of the magnetic field produced by intra-cellular currents inside the brain at up to also about 200 spatial locations. It is estimated that about 10000 neurons have to be active simultaneously to create a magnetic field that can be picked up from outside the brain even though the sensors used (so-called Superconducting Quantum Interference Devices or SQuIDs) are sensitive to magnetic fields on the order of 10 fT (femto Tesla = 10^{-15}Tesla) which is less than one billionth part of the earth's magnetic field. MEG signals generally show more spatial structure than EEG signals because the magnetic field can penetrate the tissue with very little interaction. MEG is mainly sensitive to tangential current flow because this type of current creates magnetic fields that enter and exit the head whereas radial currents have magnetic fields which are confined inside. It should be mentioned that even though only the radial component of the field is measured it is possible (at least in principle) to calculate the other two components tangential to the surface defined by the sensors using Maxwell's equations (Lütkenhöner 1994). In any case, there always exist (infinitely many)

current distributions inside a volume (the brain) that leave no signal at all in a set of sensors arranged on a surface around it; any one of them can be added to a current distribution that is compatible with the measured field, and therefore the inverse problem has no unique solution.

Both techniques have a high resolution in time (on the order of ms) and a low resolution in space (on the order of cm) due to inter-sensor distances on the head. "Low" here is with respect to techniques like MRI where the spatial resolution is on the scale of mm in a 3d volume. Nevertheless, the amount of data produced in experimental sessions is enormous as a simple estimate shows: If we record from 200 EEG and/or MEG sensors at a sampling frequency of 250 Hz and an accuracy of 16 bits we have $200 \times 250 \times 2 = 100\,000$ bytes/sec or more than a GigaByte for 3 hours of recording time. Interestingly, these numbers don't seem frightening anymore because almost two hours fit on a single CD. The more important question is how to extract the relevant information from such a dataset because even after say averaging we are still left with one time series for each sensor as shown in Fig. 1.

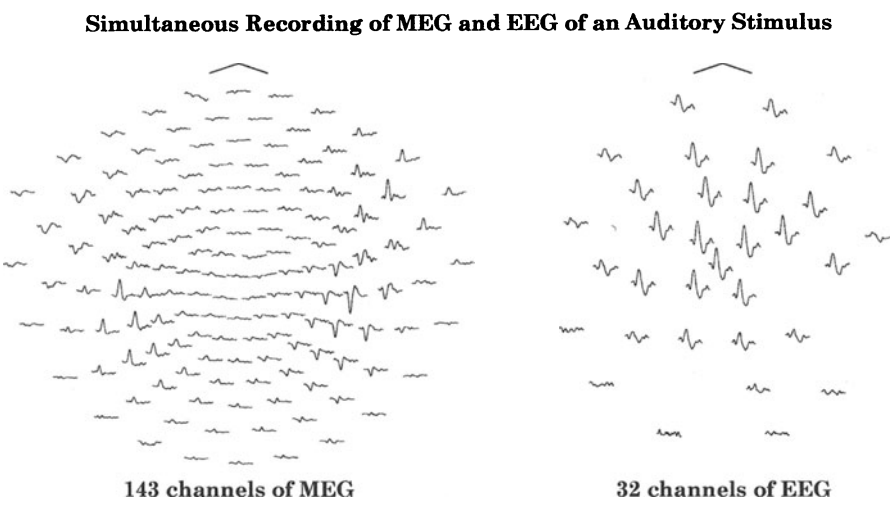

Fig. 1. Time series of a simultaneous recording of 144 channels of MEG and 32 channels of EEG for an auditory stimulus (data courtesy of CTF Inc., Vancouver)

It is evident that a great amount of the information in this dataset is redundant and plotting all these time series is certainly not the best way to visualize the spatiotemporal dynamics we are interested in. Color coded topographic maps plotted at certain timepoints can be used to show the spatial patterns for the electric potential or the magnetic field. Because the

sensors are usually not arranged on a planar surface projection procedures must be used to obtain a pattern on flat paper without loosing information from hidden sensors. The topos in this article are calculated the following way: Assuming a center in the middle of the head, the 3d (x, y, z) coordinates of the sensors can be transformed into spherical coordinates (r, θ, ϕ). The 2d coordinates for the plots are then given by

$$X = s\,\theta\cos\phi, \quad Y = s\,\theta\sin\phi \tag{1}$$

where s is a scaling factor that determines the size of the figure. An example showing the sensor locations and a pattern of neural activity on a subject's head, together with the projection and a color scale that links certain colors to magnetic field amplitude is given in Fig. 2. Figure 3 shows topographic maps from the time series in Fig. 1 at two different timepoints ($t = 108$ ms, and $t = 220$ ms after stimulus onset). These points were picked to answer the question what is the "better" technology EEG or MEG (this issue is currently fought out in the BIOMAG mailing list (which can be found on CTF's web site: http://www.ctf.com). In Fig. 3 at $t = 108$ ms, clearly, the MEG pattern shows more structures, i.e. two dipolar patterns indicating current dipoles in the left and the right hemisphere pointing posterior. The pattern of the electric potential is quite structureless. At $t = 220$ ms there is virtually no magnetic field but a strong positive potential picked up by the EEG. Of course, the scaling for the two time points is the same as indicated by the color scales. This is a situation where current flow exists inside the head but in a way that leaves virtually no traces in the SQuID sensors. Therefore, to get as much information as possible about electromagnetic brain activity one would like to have measurements of both EEG and MEG, preferably recorded simultaneously.

To visualize the dynamical nature of brain activity, topographic maps can be produced for each time point and animated as movies. Examples of such animations for different conditions for EEG and MEG (in MPEG format) can be downloaded from our web site (http://www.ccs.fau.edu).

2.2 Analysis Methods

A better understanding of what is going on in large data sets can often be achieved if the data is preprocessed in certain ways that allow for an extraction of relevant information or elimination of redundancies. Here we briefly describe two linear methods that we use for this purpose.

The Karhunen–Loève Transformation. Several names are on the market for this decomposition technique including Principal Component Analysis or Singular Value Decomposition. Essentially they all follow the same basic idea: we have time series (EEG or MEG) measured at (very) many locations in space. These time series represent spatial patterns at each time point, i.e. a spatiotemporal pattern. In principle any spatiotemporal pattern $H(\mathbf{x}, t)$ can

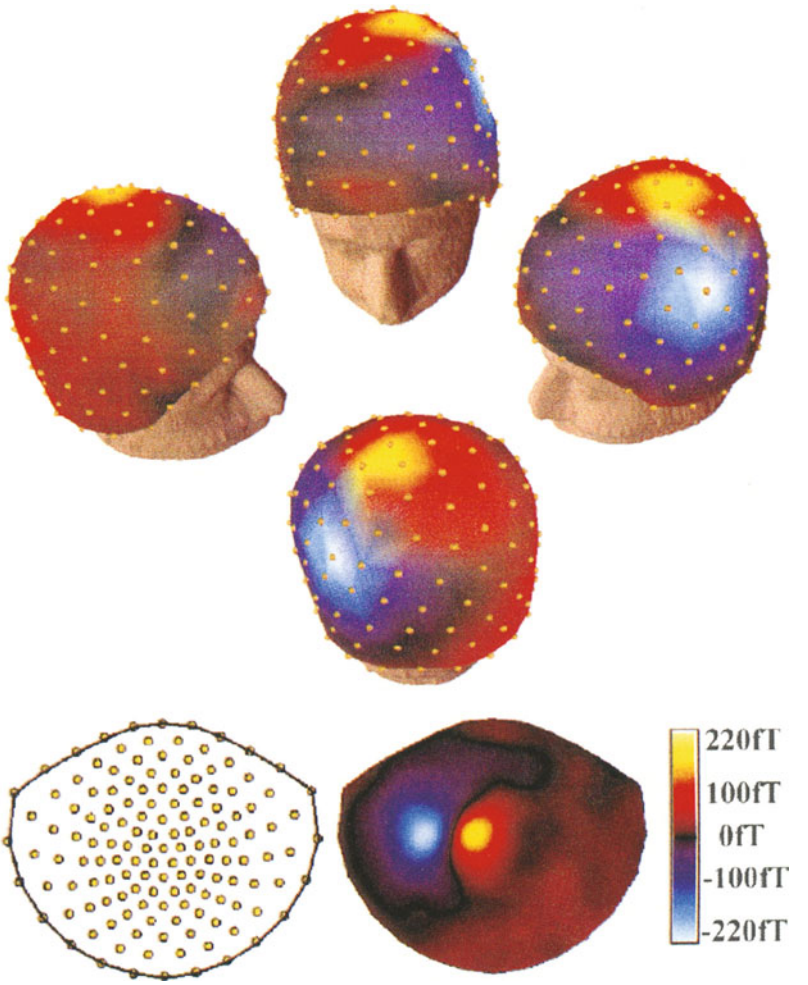

Fig. 2. A pattern of magnetic brain activity and sensor locations from four views on the subject's head (*top*), and in the projection (*bottom*). Blue indicates locations where the magnetic field is entering the head, red-yellow sites where the field is exiting the head. The color scale is in units of femtoTesla (fT)

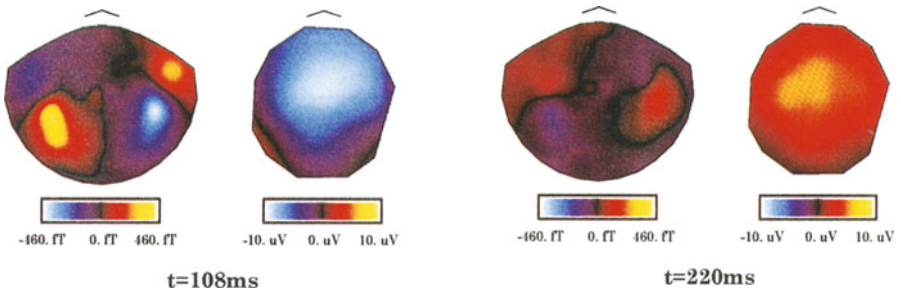

Fig. 3. Topographic maps of the data shown in Fig. 1 at two representative points in time

be written as the sum over a set of spatial patterns $\psi^{(i)}(\mathbf{x})$ multiplied by time dependent amplitudes $\xi_i(t)$:

$$H(\mathbf{x},t) = \sum_{i=1}^{N} \xi_i(t)\,\psi^{(i)}(\mathbf{x}) \; . \tag{2}$$

In our case space and time are discrete, i.e. the function $H(\mathbf{x},t)$ is known at certain locations k in space and at certain time points depending on the sampling frequency. However, in the following we assume that space is discrete but keep time continuous because it simplifies the notation. This way $H(\mathbf{x},t)$ becomes a vector $\mathbf{H}(t)$ at every time point where the component $H_k(t)$ represents the amplitude (potential difference between an electrode and the reference, or magnetic field component) at sensor location k and time t. By applying the same notation to the spatial functions $\Psi^{(i)}(\mathbf{x})$ (2) reads for component k:

$$H_k(t) = \sum_{i=1}^{N} \xi_i(t)\,\psi_k^{(i)} \; . \tag{3}$$

If the vectors $\Psi^{(i)}$ form a complete set and N is equal to the number of sensors the original signal $\mathbf{H}(t)$ is reconstructed *exactly*. The more interesting question, however, is: Can we obtain a set of vectors $\Psi^{(i)}$ for which we have to sum over only a few, say $M \ll N$, and still get a decent (90–95%) reconstruction of the original signal? It can be shown that the Karhunen–Loève (KL) transformation creates such a set of vectors $\Psi^{(i)}$ such that for *any* truncation point M, the mean square error between the original and the reconstructed signal becomes a minimum:

$$E_M = \sum_{k=1}^{N} \int_0^T \mathrm{d}t \left(H_k(t) - \sum_{i=1}^{M} \xi_i(t)\,\psi_k^{(i)} \right)^2 = \mathrm{Min}\;\forall M \; . \tag{4}$$

It can also be shown that the basis vectors $\Psi^{(i)}$ in this case are the eigenvectors of the covariance matrix $\mathbf{C}$ from the time series $h_i(t)$:

$$C_{kl} = \int_0^T \mathrm{d}t\, h_k(t)\, h_l(t) \quad \text{with} \quad h_k(t) = H_k(t) - \bar{H}_k \tag{5}$$

where $\bar{H}_k$ is the mean value of the time series from sensor k. The eigenvalues of this matrix are a measure of how much the corresponding eigenvector contributes to the variance of the original signal. Notice that the covariance matrix is symmetric and therefore its eigenvalues are real numbers and its eigenvectors are orthogonal. The time dependent amplitude $\xi_i(t)$ for the vector $\Psi^{(i)}$ is given as the scalar product between the vector and the pattern at time t, $\mathbf{H}(t)$

$$\xi_i(t) = \mathbf{H}(t)\, \Psi^{(i)} = \sum_{k=1}^{N} H_k(t)\, \psi_k^{(i)} \,. \tag{6}$$

The patterns $\Psi^{(i)}$ and the time series $\xi_i(t)$ fulfill the orthogonality relations

$$\Psi^{(i)}\, \Psi^{(j)} = \sum_{k=1}^{N} \psi_k^{(i)}\, \psi_k^{(j)} = \delta_{ij} \quad \text{and} \quad \frac{1}{T} \int_0^T \mathrm{d}t\, \xi_i(t)\, \xi_j(t) = \lambda_i\, \delta_{ij} \tag{7}$$

where δ_{ij} represents the Kronecker-delta. In the sense of (4) the set of basis vectors $\Psi^{(i)}$ is optimal which means it is not possible to find a different set of M vectors that has a smaller mean square error. There may be circumstances, however, where it is of advantage to minimize other quantities (like in the bi-orthogonal decompositions discussed below).

Figure 4 shows the first three spatial patterns and their corresponding time dependent amplitudes from a KL-expansion of the dataset from Fig. 1 for the case of EEG (top row) and MEG (bottom row). For EEG the pattern representing the first eigenvector contributes already about 97% to the variance of the signal, i.e. by using only this pattern we can get a very good reconstruction of the whole dataset – an enormous compression of information compared to the 32 time series. For MEG three patterns are necessary to account for 90% of the variance. Movies in MPEG format showing the spatiotemporal dynamics of the original signal together with a reconstruction from one, two, and three spatial patterns can be downloaded from our web site.

Bi-Orthogonal Expansions. The bi-orthogonal expansions are used to obtain a bi-orthogonal set of vectors and time dependent amplitudes calculated from a spatiotemporal pattern corresponding to a given second set of time series. Say we have a set of time series $H_k(t)$ from EEG or MEG recordings where k represents the different sensors. In addition, we have a second set of time series, $r_i(t)$, for instance the movement profile of a finger and its derivative. From these two sets we want to calculate the spatial patterns $\Psi^{(i)}$ in

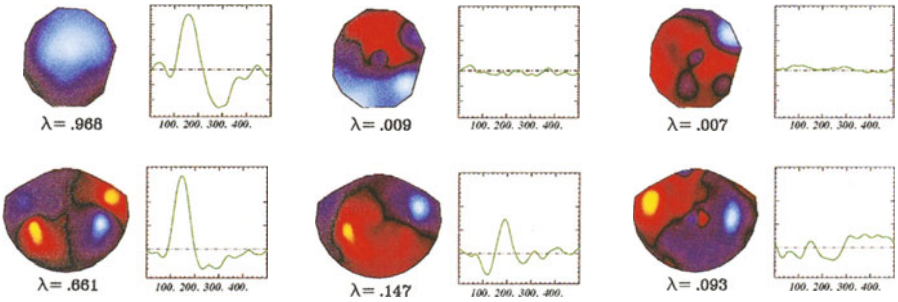

Fig. 4. Kl-expansion of the data shown in Fig. 1 (see text)

a way that if we project $\mathbf{H}(t)$ onto them we get an approximation of $r_i(t)$. There are various ways to do that:

- We can calculate the patterns according to

$$\sum_{k=1}^{N} \sum_{i=1}^{M} \int_0^T \mathrm{d}t \, \{H_k(t) - r_i(t)\, \psi_k^{(i)}\}^2 = \mathrm{Min} \tag{8}$$

  In this case the patterns can readily be calculated by taking the derivative of (8) with respect to $\psi_m^{(j)}$ and solving for $\psi_k^{(i)}$. The equations are completely decoupled and $\psi_k^{(i)}$ is given by:

$$\psi_k^{(i)} = \frac{\langle h_k(t)\, r_i(t) \rangle}{\langle r_i^2(t) \rangle} \tag{9}$$

  where $\langle ... \rangle$ is an abbreviation for the time average $\frac{1}{T} \int_0^T \mathrm{d}t \, ...$.
- A second possibility is to calculate the patterns according to:

$$\sum_{k=1}^{N} \int_0^T \mathrm{d}t \, \{H_k(t) - \sum_{i=1}^{M} r_i(t)\, \psi_k^{(i)}\}^2 = \mathrm{Min} \tag{10}$$

  Notice that this case is more like an expansion. Now, taking the derivatives with respect to $\psi_m^{(j)}$ leads to linear systems of equations of dimension M for the components $\psi_k^{(i)}$ which have to be solved for every k:

$$\langle r_j(t)\, H_k(t) \rangle = \sum_{i=1}^{M} \langle r_i(t)\, r_j(t) \rangle\, \psi_k^{(i)} \tag{11}$$

A priori it is not evident which one of these techniques is "better". In any case, the vectors $\Psi^{(i)}$ will not form an *orthogonal* basis. Therefore, a set of adjoint vectors $\Psi^{(i)+}$ needs to be calculated that fulfills the relation:

$$\Psi^{(i)+}\,\Psi^{(j)} = \delta_{ij} \quad \text{and} \quad \Psi^{(i)+} = \sum_{j=1}^{M} a_{ij}\,\Psi^{(j)} \tag{12}$$

Using these adjoint vectors the set of time series $\xi_i(t)$ corresponding to $r_i(t)$ is then obtained as:

$$\xi_i(t) = \sum_{k=1}^{N} h_k(t)\,\psi_k^{(i)+} \quad . \tag{13}$$

Friedrich and Uhl (1992, 1996) used such expansions to obtain spatial patterns that represent the dynamical properties of a data set more appropriately than the patterns obtained by the KL-expansion which are restricted by the orthogonality constraint (7). The idea is to use the time series for the dominating pattern from a KL-expansion and to calculate the other patterns in a way that they correspond to temporal derivatives of this function. This way the data can be represented by a dynamical system of first order differential equations of the form

$$\dot{\eta}_1 = \eta_2 \quad , \quad \dot{\eta}_2 = \eta_3 \quad , \quad \ldots \quad , \quad \dot{\eta}_n = f\{\eta_1, \eta_2, \ldots, \eta_n\} \tag{14}$$

where a set of two bi-orthogonal patterns relates to each variable η_i. Bi-orthogonal expansions of the second type are depicted in Fig. 5, again for the EEG (upper row) and MEG (lower row) data sets. Shown are the most dominant patterns from a KL-expansion (left most column) for EEG (top) and MEG (bottom) and the corresponding adjoint pattern (second column from left) together with the time series calculated according to (13) in red. The original time series from the KL-decomposition is also plotted in green but is not visible in this case because the two curves are virtually identical. In the fourth and fifth columns the patterns that best fit the time dependence of the derivative of the curves in column three are shown with their corresponding adjoint patterns, respectively. Again in column six the original time series (the derivatives of the curves in column 3) are plotted in green and the

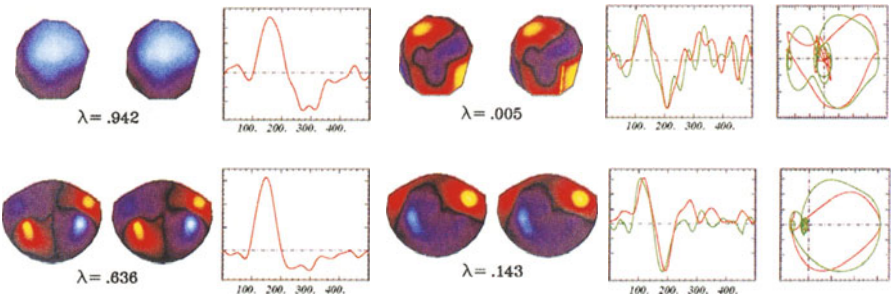

Fig. 5. Bi-orthogonal expansion of the data shown in Fig. 1 (see text)

curve reconstructed from (13) in red. In this example the patterns and their adjoints are very similar because the patterns are almost orthogonal which is not always the case. The right-most column shows phase space plots, i.e. $\xi(t)$ plotted in the x-direction and $\frac{\mathrm{d}}{\mathrm{d}t}\xi(t)$ in the y-direction. The attractors are obviously not unfolded in two dimensions since the trajectories intersect. However, the skeleton is the same for all four curves: There is one fixed point at $\xi = 0$ and there appears to be a second fixed point for a negative value of ξ. So even though the spatial patterns picked up be MEG and EEG are quite different the main features of the underlying dynamics from the viewpoint of dynamical systems are similar (for a much more sophisticated reconstruction of attractor skeletons and phase space dynamics see e.g. the contribution by Uhl et al. this volume).

3 Experimental Results

We are now going to apply the techniques outlined in the previous section to the data from the flexion-extension experiment outlined in KFJ. There we claimed that a strong correlation exists between the pattern of neural activity and the velocity profile of the finger movement for a variety of different movement directions or movement rates. In order to examine this relation further we first have a closer look at the dynamics of the movement itself (the movement amplitude as a function of time, or movement profile) and then analyze its connection to the observed patterns of brain activity in detail.

3.1 Behavioral Dynamics

The results obtained for the coordination behavior as far as timing (in terms of relative phase between stimulus and the movement) is concerned have already been discussed in KFJ (cf. Fig. 3 therein). It has been shown that the distributions of relative phase for the syncopation conditions are broader, indicating a less stable state of the system, compared to synchronization. Here we want to concentrate on the shape of the movement profile for the different conditions. Figure 6 shows the averaged movement profile together with the corresponding standard deviations for all four task conditions.
All curves are bell-shaped but show remarkable differences between the different kinematics flexion and extension. The flexion movements are shorter, steeper during the left flank when compared with the right flank, and more variable at the time of peak movement amplitude. The extension movements, on the other hand, are wider with an earlier onset in the cycle, and more symmetric with an almost constant variability. If our claim stated in KFJ about the relation between brain activity and movement velocity is valid, these differences must be visible in the MEG data, i.e. we expect that the dipolar pattern of movement activity is visible in the extension conditions before it can be seen in the flexion conditions due to the wider profile of the movement.

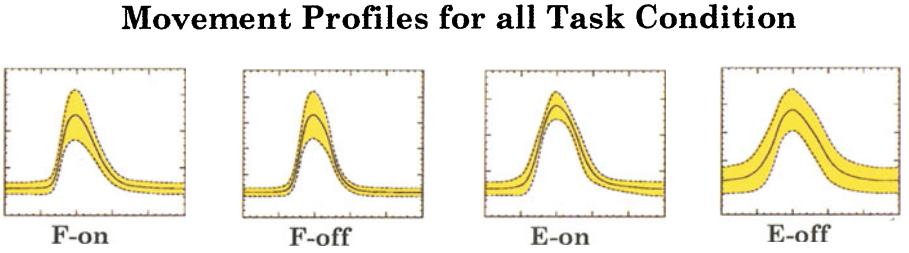

Fig. 6. Shape of the averaged movement profile with the standard deviation (shaded) for all task conditions

A movie at our web site shows this is indeed the case. It can also be seen in Fig. 4 in KFJ in which the dipolar structure becomes first visible in the row $t = -120$ ms for the extension and at $t = -60$ ms for the flexion movement.

3.2 Brain Dynamics

To examine the relation between movement velocity, $v(t)$, and the brain signal in sensor k, $H_k(t)$, the cross correlation at zero time lag, $C_k(\tau = 0)$, was calculated as

$$C_k(\tau) = \frac{\langle \{H_k(t) - \langle H_k(t) \rangle\} \{v(t) - \langle v(t) \rangle\} \rangle}{\sqrt{\langle \{H_k(t) - \langle H_k(t) \rangle\}^2 \rangle \langle \{v(t) - \langle v(t) \rangle\}^2 \rangle}} \,. \tag{15}$$

Figure 7 shows its value color coded as a function of space. Note that at the locations of maximum field magnitude (see Fig. 4 KFJ) the cross correlation is close to ± 1 indicating strong correlations or (anti-correlations) between movement velocity and magnetic brain activity. Figure 8 shows an overlay of the time series at sensor locations (green) and movement velocity (red; note the velocity profile is multiplied by the corresponding correlation value to correct for the fact that due to the dipolar nature of the pattern, the signal

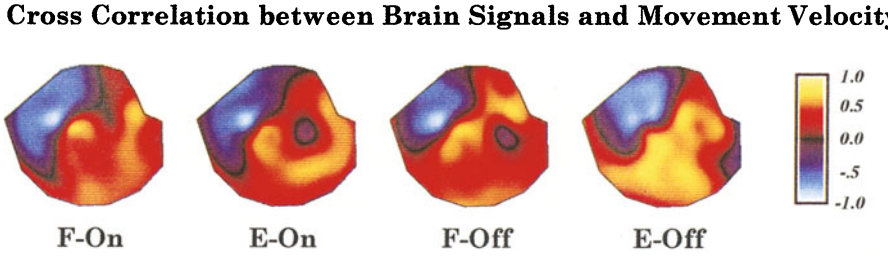

Fig. 7. Cross-correlation as a function of space for all task conditions

is reversed in some of the sensors). Within the highlighted region (where the field maximum and minimum is located), the time series of these two quantities match extremely well.

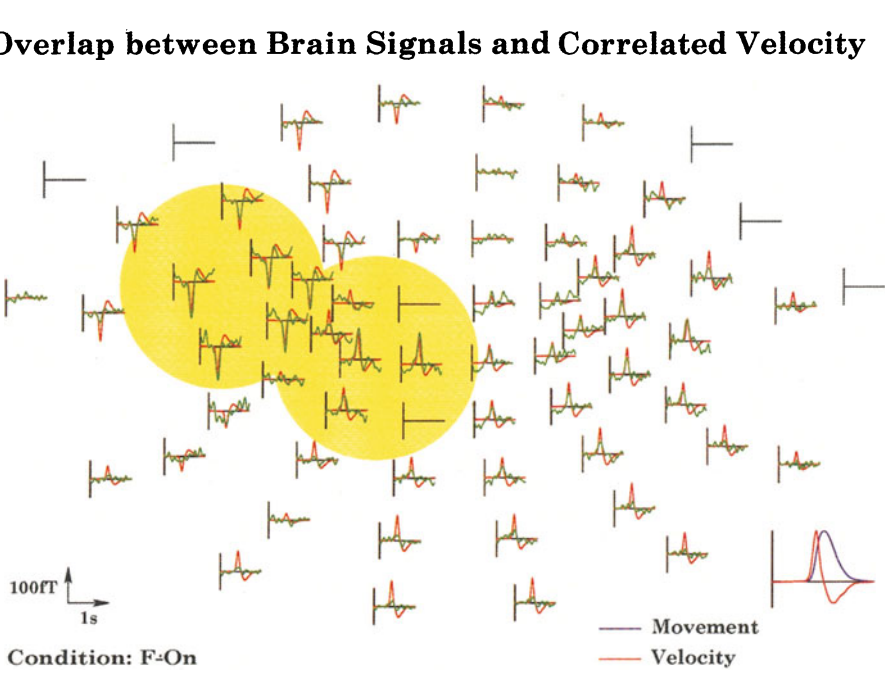

Fig. 8. Overlap between brain signals in all sensors (green) and the correlated movement velocity, i.e. the product of the velocity and the cross-correlation value $C_k(\tau = 0)$ in the sensor (red). This quantity was chosen, because due to the dipolar nature of the magnetic field patterns, the signals in some sensors are reversed versions of the signal in others. In the highlighted region these correlation values are close to ± 1 as shown in Fig. 7

As described earlier, the decomposition of a spatiotemporal pattern into a spatial part (consisting of static spatial patterns $\psi^{(i)}(\mathbf{x})$) and a temporal part (consisting of a time series, i.e. amplitudes corresponding to the different patterns at each time point) can lead to a drastic compression of information. How many patterns one has to take into account in order to get a decent reconstruction of the original signal depends on the data set under consideration. As seen above for the case of an auditory evoked response in EEG we needed only one pattern to account for over 95% of the variance in the original signal whereas for the case of MEG at least 3 patterns were necessary (if the original data set is purely random in space and time no reduction at all is achieved with these techniques).

In KFJ it has been shown that the time dependent amplitude corresponding to the dominating pattern from a KL-expansion approximates the shape of the movement velocity profile quite well for all task conditions (see Fig. 5 in KFJ). The time series for the second mode has no obvious interpretation due to the orthogonality constraint (7). Therefore, we applied the second of the bi-orthogonal expansions described in the previous section to the data and calculated the set of bi-orthogonal patterns corresponding to both the movement profile amplitude and velocity. Figure 9 shows the decompositions of the spatiotemporal brain signal for the four task conditions.

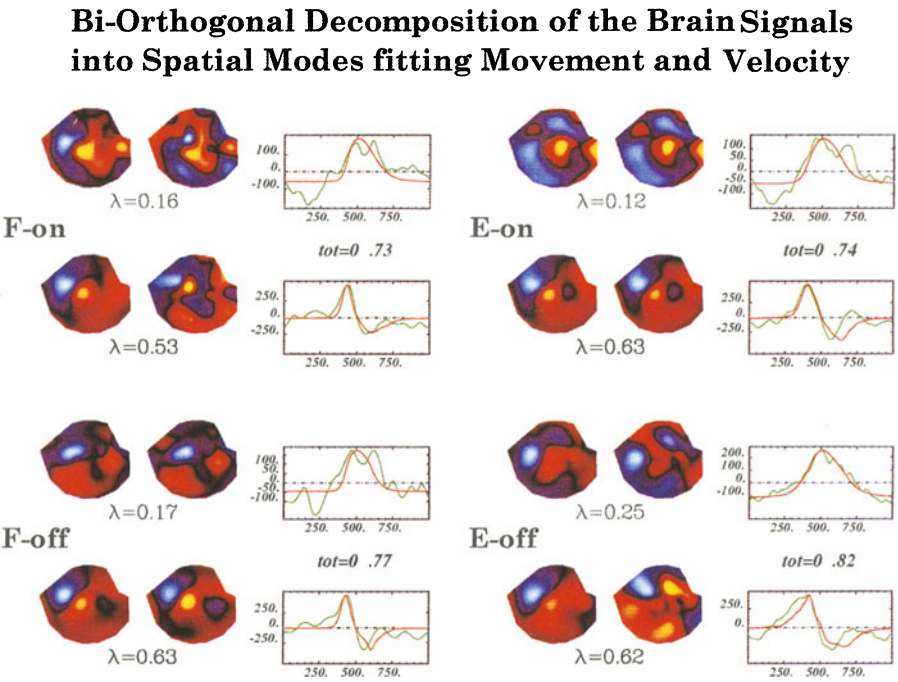

Fig. 9. Decomposition of the data using the second bi-orthogonal expansion. For each condition the upper patterns represent the modes $\Psi^{(1)}$ and $\Psi^{(1)+}$ corresponding to the finger displacements while the lower patterns $\Psi^{(2)}$ and $\Psi^{(2)+}$ relate to movement velocity. The values of λ are an estimate of the contribution of these modes to the variance of the original signal. On the right, the time series of the averaged displacement (red, top) and its temporal derivative, the finger velocity (red, bottom), are plotted for each condition. The green curves represent the projection of the original brain signal onto the adjoint vectors, i.e. the time-dependent amplitudes $\xi_1(t)$ and $\xi_2(t)$ from a reconstruction of the signal according to (3). The value of *tot* is an estimate of the quality of the reconstruction if both modes are used

Two remarks have to be made here: First, the two λs in general do not add up to the total contribution (as they do for the KL-expansion) because the patterns are no longer orthogonal and therefore some contributions of one pattern can be canceled by contributions from the other pattern. The decomposition only makes sense if the angle between the first and the second pattern (given by their scalar product) is not too small (estimates say at least 30°). Second, the quality of the reconstruction in terms of least square error can not be better than the reconstruction from the first two KL-modes (in fact, the fit is worse in all cases where the bi-orthogonal set of patterns are not the same as those obtained from the KL-expansion). In some sense we are trading here accuracy of the fit against functional relevance of the patterns, because now these vectors can be interpreted in terms of the behavior: They are the spatial patterns of the magnetic field produced by the neural activity that best follows the time course of movement amplitude and movement velocity - functionally relevant quantities created by the human motor system. The quality of the reconstruction from these two modes is still excellent as can be seen in Fig. 10 showing an overlay of the original (green) and the reconstructed brain signal (red).

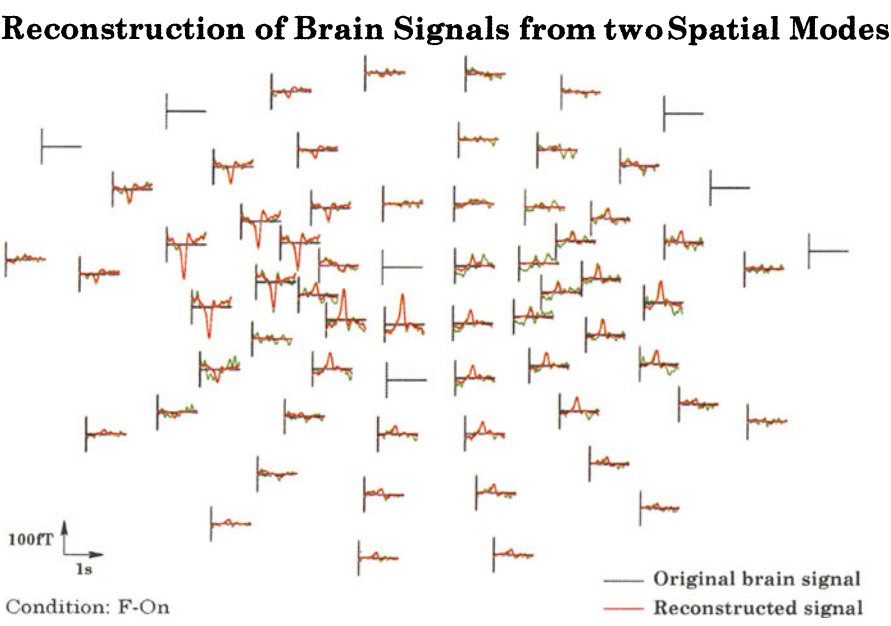

Fig. 10. Reconstruction of the signal from the two spatial patterns corresponding to movement amplitude and movement velocity

So far we have seen that the brain signals are very similar for the four different task conditions, i.e. independent of movement direction or coordi-

nation requirements. Specifically, the spatiotemporal patterns corresponding to both movement amplitude and velocity are dominated by a strong dipolar structure over motor cortex in the left hemisphere. After demonstrating these similarities we now ask the question: Can we find differences? Due to their large amplitudes, the motor-related patterns mask any differences that might exist between task conditions. Therefore, we first remove them by subtracting the contribution of both patterns at each point in time. In other words we subtract the red curves from the green curves (Fig. 10) and calculate the residual patterns for each condition separately. Figure 11 shows the results from this procedure.

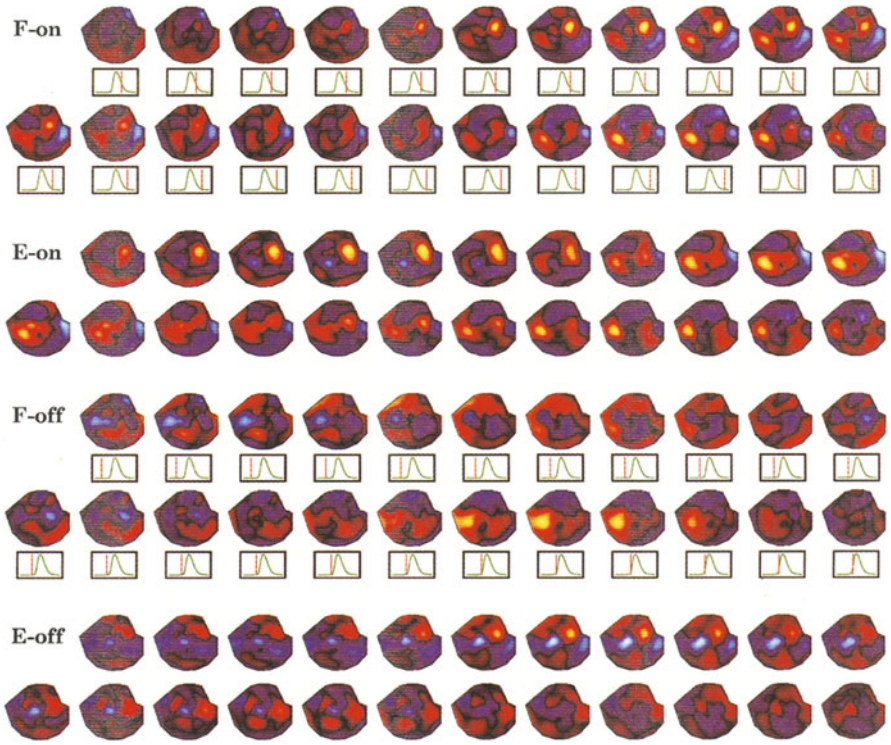

Fig. 11. Residual patterns after the dominating motor-related activity is removed for all task conditions at certain locations within a cycle (see text for details)

We are looking for dynamical structures that are similar in different conditions and occur at about the same time within the cycle. The top two rows show a sequence of topographic maps from the flexion-on condition occurring after peak movement as indicated in the boxes below each pattern. From left to right in the top row a red-yellow structure, indicating magnetic field that

exits the head, appears over right frontal areas followed by activity of the same polarity over left central areas a little later in the cycle. In the second row this pattern of activity almost vanish before the left central structure reappears. A very similar scenario can be seen in the third and fourth rows which show the spatial patterns from the extension-on conditions at the same time points. The right frontal activity appears a little earlier in the cycle but the sequence is the same and the left central activity disappears at the same time in both conditions. For the off-the-beat conditions no such structure is observable after peak movement (not shown). However, if we look at time slices that are shifted by half a cycle with respect to the patterns shown for the on-the-beat conditions we find the two pattern sequences displayed in the bottom rows. Given the time shift, the left central activity in the flexion-off shows approximately the same time course observed in in the on-the-beat conditions. Similar observations can be made for the activity over right frontal areas in the extension-off condition. These similarities are probably due to the fact that the pattern sequences are now stimulus locked in all conditions. However, it is not easy to explain them because the stimulus in this experiment was a small LED and control conditions revealed no evoked visual fields. Therefore, it is likely that these sequence are related to some higher level processing of the stimulus. The most interesting point here is that in the off-the-beat conditions only parts of the sequence exists which could mean that the rest is annihilated by other ongoing activity and one may speculate that the instability of the syncopic coordination is related to these interferences.

4 Conclusions and Outlook

The main point in this paper was to show how visualization and analysis techniques can be used to extract relevant features from large sets of experimental data. Relevant here means features that link neural activity patterns on one level and human behavior, in this case motor behavior in a coordination experiment, on another level. It takes the coherent action of tenthousands of neurons to produce a signal that we can measure from outside the head or to make a finger move, but it is the movement of the finger on the other hand that leads to the coherent neural activity. This is the kind of circular causality which is present in all systems showing self-organization, and explored in the theory of synergetics founded by Hermann Haken. We can substitute "atoms" for "neurons" and "laser light" for "finger movement" because the same basic laws of self-organization govern the dynamics of entirely different systems. The hope is thus that some day we will be able to understand brain function as well as we understand the laser. To achieve this goal, both experimental and theoretical investigations are needed. Experimentally, performing the movement at different coordination frequencies should tell us whether or not the sequence of the stimulus related activity in the off-the-beat condi-

tions is longer at lower frequencies, shrinks when the frequency is increased and eventually vanishes when syncopation becomes unstable. From theory we could learn what kind of nonlinear interactions lead to such an annihilation process and where in the cortex the sources of activity must be located to create the observed activity patterns. The high spatial resolution of functional MRI could be used to identify these regions. Once known, together with high resolution EEG and MEG measurements, a combination of experimental data and knowledge about dispersion and propagation properties of the neural tissue (including inhomogeneities) could eventually lead us to a "solution" of the inverse problem after all.

Acknowledgements

We thank Tom Holroyd for help with data collection and Justine Mayville for her help in the final stages of the manuscript. This research was supported by NIMH (Neurosciences Research Branch) Grant MH42900, KO5 MH01386 and the Human Frontiers Science Program. VKJ gratefully acknowledges a fellowship from the *Deutsche Forschungsgemeinschaft.*

References

Friedrich, R., Uhl, C. (1992): Synergetic Analysis of Human Electroencephalograms: Petit-Mal Epilepsy. In *Evolution of Dynamical Structures in Complex Systems*, Friedrich, R., Wunderlin, A., eds., Springer, Berlin, Heidelberg

Friedrich, R., Uhl, C. (1996): Spatiotemoral Analysis of Human Electroencephalograms: Petit-Mal Epilepsy. Physica D 98, 180

Fuchs, A., Kelso, J.A.S., Haken, H. (1992): Phase transitions in the Human Brain: Spatial Mode Dynamics. Int. J. Bifurc. Chaos 2, 917-939

Le, J., Gevins, A. (1993): Method to Reduce Blur Distortion from EEGs using a Realistic Head Model, IEEE Trans. on Biomed. Eng. 40, 517-528

Jirsa, V.K., Haken, H. (1996): Field theory of electromagnetic brain activity. Phys. Rev. Let. 77, 960–963

Jirsa, V.K., Haken, H. (1997): A derivation of a macroscopic field theory of the brain from the quasi-microscopic neural dynamics, Physica D 99, 503–526

Lütkenhöner, B. (1994): The magnetic field arising from current dipoles randomly distributed in a homogenous spherical volume conductor. J. Appl. Phys. 75, 7204-7210

Meaux, J.R., Wallenstein, G.V., Nash, A., Fuchs, A., Bressler, S.L., Kelso, J.A.S. (1996): Cortical Dynamics of the Human EEG Associated with Transitions in Auditory-Motor Coordination. Society for Neuroscience Abstracts Vol. 22/2, 890

Nunez, P.L. (1981): *Electric fields of the brain*, Oxford University Press

Law, S.K., Nunez, P.L., Wijesinghe, R.S. (1993): High-Resolution EEG Using Spline Generated Surface Laplacians on Spherical and Elliptical Surfaces. IEEE Trans. Biomed. Eng. 40, 145–153

Wallenstein, G.V., Kelso, J.A.S., Bressler, S.L. (1995): Phase transitions in spatiotemporal patterns of brain activity and behavior. Physica D 84, 626-634